Chinese Journal of Physics 70 (2021) 343–354

Contents lists available at ScienceDirect

Chinese Journal of Physics

journal homepage: www.sciencedirect.com/journal/chinese-journal-of-physics

Topological information in artificial spin ice with random vacancies

F. Brevis [a], P. Díaz [*,a], D. Laroze [b], L.M. Pérez [b,*], E.E. Vogel [a,c]

[a] Departamento de Ciencias Físicas, Universidad de La Frontera, Temuco, Chile
[b] Instituto de Alta Investigación, CEDENNA, Universidad de Tarapacá, Casilla 7D, Arica, Chile
[c] Center for the Development of Nanoscience and Nanotechnology, CEDENNA, Santiago, Chile

ARTICLE INFO

Keywords:
Artificial spin ice
Vertex types
Random vacancies
Time correlation
Magnetic memory

ABSTRACT

In this work, we perform a numerical study on artificial spin ice systems formed by square arrays of ferromagnetic nano-islands. Inspired by topological studies, we consider absent nano-islands at random positions throughout the array. The system is described by a Hamiltonian that includes anisotropy energy as well as dipolar interaction among the islands in the Heisenberg spin model approach. The simulations were done in the framework of the Monte-Carlo method with the Metropolis algorithm. We focus on the effect of the vacancies on the magnetic vertices configurations. In particular, we calculate the distribution of all possible magnetic configurations of the vertices as a function of the percentage of vacancies. The absent nano-islands generate a loss of geometric frustration, and the system evolves faster than the system without vacancies to a lower energy state. However, the system shows the difficulty of reaching the ground state because the vacancies generate different sub-regions that evolve towards one of the two possible orientations of the magnetic moments with the minimum energy state. Furthermore, we show this system to be stable up to room temeperature when a state with local minimal energy is initially considered. Consequently, the system retains its information in a wide range of temperatures. The introduction of vacancies breaks with any translational symmetry and allows diversifications of the number of magnetic configurations with minimum energy. Therefore, this kind of systems can be used to store information.

1. Introduction

The study of frustration in magnetic systems has led to a wide variety of experimental and theoretical studies in recent decades [1–4]. The distinction between spin glass frustration and geometric frustration was systematically exposed by Ramirez et al., where two and three dimensional magnetic systems in which geometric frustration is observed were presented [5]. In particular, complex magnetic molecules in which each spin is located at the corners of a tetrahedron, were among the first candidates to observe geometric frustration, since no configuration satisfies all interactions between the spins simultaneously. The first evidence of frustration in ferromagnetic systems was found in the ferromagnetic pyrochlore $Ho_2Ti_2O_7$, in which frustration arises from the mixture of ferromagnetic interactions and single-ion anisotropy [6]. This local anisotropy connects the spins with the center of the tetrahedron, such that the fundamental state is obtained with two spins going in and two spins coming out. This phenomenon is analogous to the ice rules

* Corresponding author.
E-mail addresses: pablo.diaz@ufrontera.cl (P. Díaz), lperez@uta.cl (L.M. Pérez).

https://doi.org/10.1016/j.cjph.2021.01.005
Received 30 April 2020; Received in revised form 4 January 2021; Accepted 13 January 2021
Available online 3 February 2021
0577-9073/© 2021 The Physical Society of the Republic of China (Taiwan). Published by Elsevier B.V. All rights reserved.

considered for the order of protons in water ice [7]. There are six magnetic configurations for the minimum energy state, which implies the existence of a residual entropy that characterizes what is called the Ice Regime. This is how the Spin Ice model was born. The validation of this correspondence was given by calculating the entropy of pyrochlore titanate $Dy_2Ti_2O_7$, which turned out to be similar to the value given for water ice [8]. Pauling introduced the concept of the *macroscopically degenerate ground state*, and this idea was directly passed to the Spin Ice.

A new impulse to the study of geometrically frustrated magnetic systems was the work done by Wang et al. [9]. The authors found that a square array of elongated islands of ferromagnetic material manufactured by lithography can emulate spin ice. In this experimental setup, the directions of the island axes form a square lattice, such that the directions of four islands converge at the lattice points, which is similar to the point of convergence of the spins in the tetrahedron of the pyrochlores. The magnetic shape anisotropy of the islands results in an Ising-like behavior of their magnetic moments, such that the dipole interaction between islands cannot be satisfied simultaneously. Consequently, it generates geometric frustrations. This arrangement of magnetic islands is called *Artificial Spin Ice* (ASI). From an experimental point of view, the ASI gives an important advantage by having macro-spins as fundamental units whose magnetization is possible to be observed directly through different experimental techniques. Some of these techniques are low-energy muon spectroscopy [10], resonant magnetic x-ray photon correlation spectroscopy [11], and magnetic force microscopy [12,13], to mention a few. In ASI, there is a critical temperature associated with the magnetostatic interaction among the islands in which the system freezes, as it is shown in Ref[11]. More recently, a detailed study was carried out on how the size of the islands influences thermal annealing [14]. Besides, in Kagome arrays, progress has been made in thermalization and the search for the fundamental state of quasi-crystal arrays [12].

Let us remark that the mimicry with natural systems is not total. For example, in the case of a square array, the distances between the islands at a vertex are not the same, unlike what is observed in the tetrahedral configurations of pyrochlores. This difference generates that the magnitude of the interaction between the magnetic moments is also different. The discrepancy causes a split in the energy of the six configurations that comply with the ice regime, leaving only two possible configurations in the fundamental state, which breaks the degeneration observed in natural crystals. This problem was tackled several years later by producing two square sublattices on different planes [15], and incorporating a disk at the vertex that modifies the interactions between the islands [16]. More recently, it has been shown that for rectangular lattices, it is possible to observe very similar thermodynamical behavior to the ice regime [13]. Beyond this discrepancy, thermodynamical models of square ASI were discussed early on [17], evidencing the problem of thermal activation and the difficulty of artificial systems to evolve towards the fundamental state. The collective dynamics of ASI arrays were experimentally verified in 2011 [18], and significant advances were further developed in Ref. [19].

The topological order began to be the subject of discussion because they reveal a richness in the manipulation of the magnetic states [2,20]. A first review of the topic can be found in Ref. [1]. This review shows a diversification in the designed topologies, and of the characterization of the magnetic dynamics. An important part of the study focused on the break of the ice regime. This break generates an imbalance between the number of magnetic moments pointing towards the vertex to those pointing away from the vertex: this difference can be interpreted as magnetic monopoles [1]. A further study in a Kagome array showed that the critical temperature at which phase transitions appear could be controlled with the distance among islands [10]. In particular, it was demonstrated that the phase transitions occur at lower temperatures when the distances among the islands are higher.

Let us also comment about the technological applications of Spin Ices. An example in square arrays has been the characterization and control of magnetic monopoles [21–23]. Especially, to examine the possibility of controlling the movement of the monopoles in analogy with electronics [23]. Moreover, several works show significant advances in manufacturing techniques that include three-dimensional systems [24–27] or in the design of ASI systems for computing purposes [28–31]. Another notable application is magnetotransport through connected ASI systems, in which the array topology and the state of magnetization strongly influence the magnetoresistance [32]. At this point, the idea arises that ASIs are metamaterials in the sense that their collective properties can be designed [33]. Further developments on artificial spin ice can be found in Refs. [34–43].

The flexibility given by the nanofabrication techniques allows to dilute any crystalline structure by discarding magnetic islands in arbitrary positions [44–46]. The absence of an island is called *vacancy*. Furthermore, a square lattice with random vacancies (or decimations) limited to one vacancy per vertex, i.e. a maximum of 25% of vacancies, has been recently considered [45]. The authors demonstrated the fragility of the ice regime when considered as absent islands. The present work performs an extension of Ref. [45]. In particular, we study the effect of the vacancy on a square ASI system, such that the vacant islands have random positions. In this situation, the system will lose symmetry and consequently can break the ice regime. The main novelty is deemed to have different percentages of unoccupied islands without any restrictions, i.e., no limitations on the number of vacancies per vertex. This generalization allows new types of vertices. Our objective is to quantify the vacancy's influence on the loss of geometric frustration and how this loss impacts on the dynamics of the system. Since several new vertex states appear, we define an alphabet associated with magnetic configurations at the vertices. The types of vertices that arise in this system are similar to those in the Tetris lattice [46]. Our goal has been to explore the possibility of using this type of alphabet as a magnetic information storage system. Unlike a rewritable ASI system with an MFM equipped with a 2D vector magnet [47], we are interested in a system with the protected topological information, such that it can be stored in the lowest energy configuration. One problem that can appear is the loss of information due to thermal fluctuations. Hence, to study the robustness of the vacancy's effect, we analyze the stability of these configurations as a function of temperature. We find that despite the loss of geometric frustration, the stored patterns can be distinguished for a wide range of temperatures.

The manuscript is arranged as follows: in Section 2 we present the theoretical model of the system and indicate the methodological procedure. Also, we introduce the description of the types of vertices and the symbols associated to them. In Section 3, we compare the dynamics of a system with and without vacancies, we show the distribution of the vertices for different percentages of vacancies. In

Section 4, we show the evolution of the correlations and the thermal effects on a minimum energy pattern. Finally, the conclusions are provided in Section 5.

2. Theoretical model

We studied an ASI system composed of a square array of $n \times n$ ferromagnetic nano-islands that behave like nano-magnets. For the sake of simplicity, we will refer to them as islands. The number of sites (positions for island depositions) on the lattices, N, is related to the vertices which for sites describing a square lattice yields $N = 2n(n+1)$. The schematic representation of the system is shown in Fig. 1, such that up to four islands can converge at a point called a *vertex*. We consider the possibility that not all sites in the arrangement are occupied by an island, such that we will refer to unoccupied sites as *vacancies*. When there are vacancies, the number of magnetic islands will be lower than N, but the number of vertices remained fixed as $n \times n$.

For the theoretical description, each island is considered as a mono-domain, that means it is a macrospin approximation. In particular, we use the Heisenberg model in which the magnetic moments are vectors whose norm is conserved and can coherently rotate. The Hamiltonian includes dipole-dipole interaction as well as anisotropies for each island. Under these considerations, the Hamiltonian can be written as

$$\mathscr{H} = \sum_{i=1}^{N}\sum_{k=1}^{3} K_{i,k} m_{i,k}^2 + \frac{\mu_0}{4\pi}\sum_{i=1}^{N}\sum_{j>i}^{N}\left[\frac{\vec{m}_i \cdot \vec{m}_j - 3\left(\vec{m}_i \cdot \hat{r}_{ij}\right)\left(\vec{m}_j \cdot \hat{r}_{ij}\right)}{r_{ij}^3}\right], \tag{1}$$

where $\vec{m}_\alpha$ is the magnetic moment of the island α, r_{ij} is the distance between the positions of the $i-$ th and j-th islands, $K_{i,k}$ are the anisotropy constants of the island i such that the subindex k denotes the axis-direction ($k = x,y,z$). Each magnetic moment is expressed as $\vec{m}_\alpha = M_S V \hat{S}_\alpha$, where M_S is the saturation magnetization of the material, V is the volume of the island and $\hat{S}_\alpha$ stands for the unitary direction of the magnetic moment. In general, the anisotropy constant associated with an axis in a parallelepiped-shaped magnet has the form $K_k = \frac{1}{2}\mu_0 \mathscr{N}_k$, where $\mathscr{N}_k$ is the demagnetization factor. To calculate the anisotropy constants, one can use the analytical results of demagnetization factors presented in Ref. [48].

For our simulations, we have used the geometric characteristics of the system presented in the experimental work of Morley et al. [11]. We considered the islands as perfect solid parallelepipeds of $70 \times 30 \times 8$ nm^3, and made of Permalloy ($Ni_{80}Fe_{20}$) with a saturation magnetization $M_S = 860$ kA/m, which critical temperature is $T_C \approx 870$ K. In the array, the characteristic distance between the centers of the adjacent islands is $a = 240$ nm (see Fig. 1). For all cases, we considered an array of 24×24 vertices on a square lattice with $N = 1200$ lattice sites. Under this condition, the values of the demagnetization factors are $\mathscr{N}_x = 0.0869$, $\mathscr{N}_y = 0.2105$ and $\mathscr{N}_z = 0.7026$. Notice that with these parameters, K_z is much larger than K_x and K_y. Therefore, in a first approximation, it is possible to consider only the values in the plane. Consequently, the Hamiltonian is reduced to

$$\mathscr{H} = -\mathscr{A}\sum_{i=1}^{N/2} S_{i,x}^2 - \mathscr{A}\sum_{i=N/2+1}^{N} S_{i,y}^2 + \mathscr{E}_d \sum_{i=1}^{N}\sum_{j>i}^{N}\left[\frac{\hat{S}_i \cdot \hat{S}_j - 3\left(\hat{S}_i \cdot \hat{r}_{ij}\right)\left(\hat{S}_j \cdot \hat{r}_{ij}\right)}{d_{ij}^3}\right], \tag{2}$$

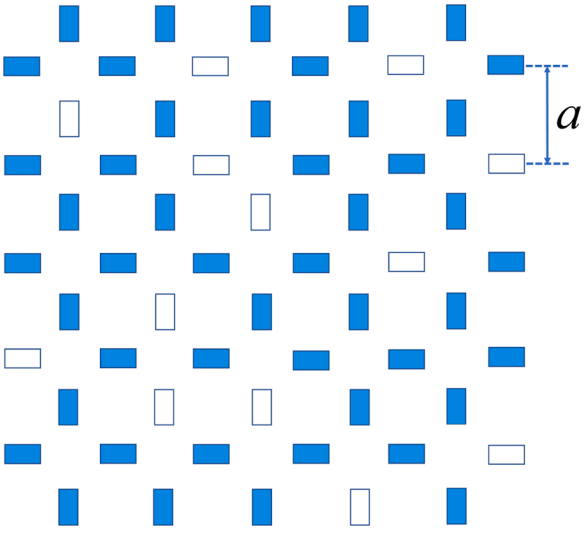


Fig. 1. Illustration of a square lattice of 5×5 vertices with 60 lattice sites. The light blue and white rectangles represent islands and vacancies respectively. (For interpretation of the references to colour in this figure legend, the reader is referred to the web version of this article.)

where $\mathscr{A} = \frac{1}{2}\mu_0(\mathscr{N}_y - \mathscr{N}_x)M_S^2$ is the effective anisotropy constant, $\mathscr{E}_d = \mu_0 V^2 M_S^2/4\pi a^3$ is an effective energy constant related to the dipole-dipole interaction strength, and $d_{ij} = r_{ij}/a$. For the selected material [11], these constants are $\mathscr{A} = 6.02$ eV and $\mathscr{E}_d = 9.44$ meV. Note that in the anisotropy energy, now the first term corresponds to the islands oriented in the x-direction (horizontal), while the second one to the islands oriented in the y-direction (vertical).

Besides, to analyze the evolution of magnetic configurations we use Monte Carlo (MC) simulations with the standard Metropolis algorithm, such that in a MC change attempt a randomly chosen moment $\widehat{S}_i$ is rotated with a uniform probability distribution in a unit sphere [4]. This move is accepted or rejected according to the probability $p = 1$, if $\Delta\mathscr{H} > 0$, or $p = \exp(-\Delta\mathscr{H}/k_BT)$, if $\Delta\mathscr{H} < 0$, where $\Delta\mathscr{H}$ is the change in energy and k_B Boltzmann's constant. Here, we have run up to 1×10^6 MC steps in most of the cases, except in some cases where the system goes fast to the thermal equilibrium states. All statistical quantities presented in the manuscript have been computed as averages over 10 independent initializations. In most of the simulations we fix the temperature at $T = 200$ K. However, in the final part of our work, we discuss the thermal effects on the system in a temperature range between 150 K and 400 K.

Finally let us comment that we consider several percentages of vacant islands, in relation to the total number of sites N, located randomly across the array. The panels (a) and (b) of Fig. 2 show the system without and with vacancies, respectively. Initially, we consider no restrictions on the number of vacant islands per vertex, which implies that it is possible to find absent vertices.

2.1. Vertex types

Due to the vacancy's effect, new kinds of vertices can be formed. In particular, the minimal number of elements can vary from four islands to zero, depending on the number of vacancies. Fig. 3 shows all types of vertices from an energetic point of view, with the corresponding notation. The digit in front of the letter V gives the number of vacancies, and the second digit gives information on the relative energy position, from bottom to top. For example, 1V-2 represents the type of vertex with a single vacancy and which is the second in increasing energy order. We have five vertex groups: 0V, 1V, 2V, 3V, and 4V. The group 2V has two possible subclasses: one L-shaped and one line-shaped. To simplify the notation, we have grouped them in increasing order of energy without distinction of the form. However, the types 2V-1 and 2V-4 correspond to the L-shaped subclass and the types 2V-2 and 2V-3 to the line-shaped subclass. Note that in the case without vacancies, only four types of vertices can be found [9], denoted by 0V. Here, new classes of vertices are incorporated.

In the case of simplest system with a maximum four islands, the normalized dipolar energy associated to the vertices are the following: $\epsilon_{0V-1} = -1.000$, $\epsilon_{0V-2} = -0.308$, $\epsilon_{0V-3} = 0.000$, $\epsilon_{0V-4} = 1.617$; $\epsilon_{1V-1} = -0.500$, $\epsilon_{1V-2} = -0.154$, $\epsilon_{1V-3} = 0.808$; $\epsilon_{2V-1} = -0.327$, $\epsilon_{2V-2} = -0.154$, $\epsilon_{2V-3} = 0.154$, $\epsilon_{2V-4} = 0.327$. These configurations are the same as those found in the tetris lattice [46], but the vertices are distributed randomly in our case. On the other hand, we must point out that each level of energy is degenerated. For example, the degeneracy for 0V-1 is 2, for 0V-2 is 4, for 0V-3 is 8 and for 0V-4 is 2.

3. Number of vacancies without restrictions per vertex

Let us analyze the system with vacancies distributed randomly across the array without considering restrictions on the number of absent islands per vertex. First, we examine the vertex distribution according to the number of vacancies for several percentages of vacant islands (PV): 10%, 20%, 30%, 40%, and 50%. This result is shown in Fig. 4. We have averaged over 1×10^3 samples with different spatial distributions of the vacancies for each percentage of vacancies. It can be seen that the vertices with most vacancies are the most numerous as the percentage of vacancies increases, i.e. when the lattice is diluted. For example, until PV= 20%, the amount of complete vertices is the highest, whereas for PV= 30% are the vertices with one vacancy, and for PV= 50% are the vertices with two vacancies. The vertex distribution, according to the number of vacancies, is decisive in the distribution of the types of vertices provided in Fig. 3.

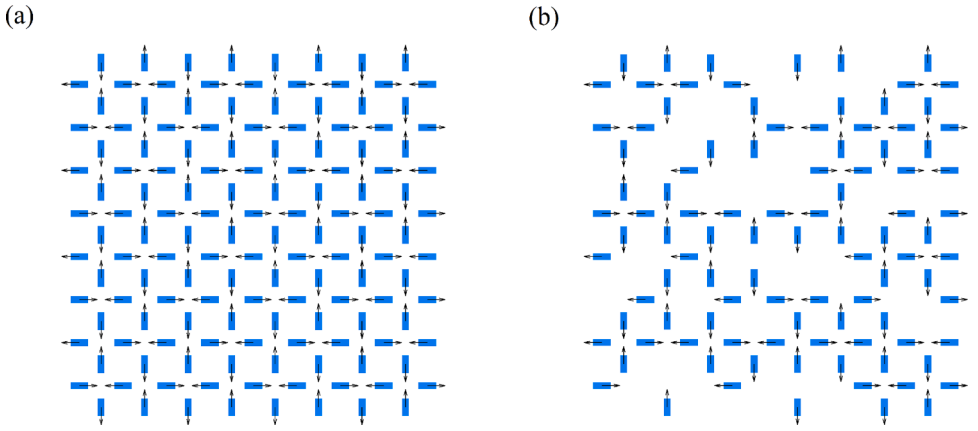


Fig. 2. Representation of a 8×8 lattice with (a) no vacancies and (b) with a 30% of random vacancies. The initial condition is the type 0V-1.

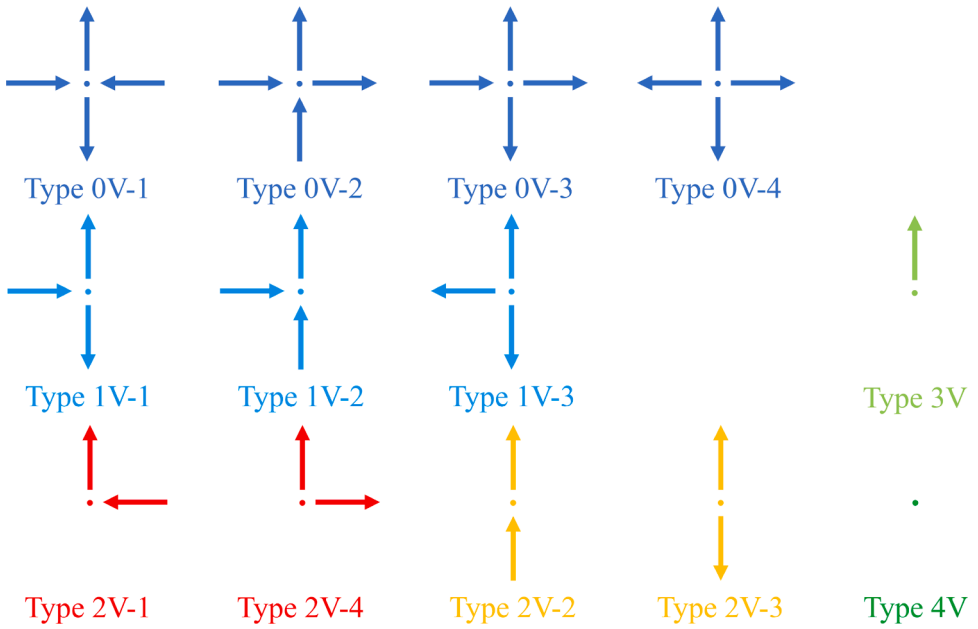


Fig. 3. Types of vertices for a square lattice of ASI. The digit in front of the letter V (for vacancy) gives the number of vacancies, and the second digit gives information on the relative energy position, from bottom to top.

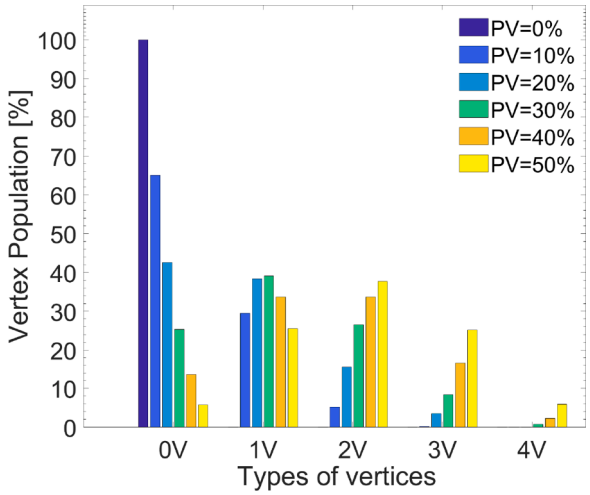


Fig. 4. Vertex distribution according to the number of vacancies for five percentages of random vacancies: 10%, 20%, 30%, 40% and 50%. The notation is the following: 0V no vacancy (full vertex), 1V one vacancy, 2V two vacancies, 3V three vacancies and 4V four vacancies (not present vertex).

3.1. Temporal evolution

We will now proceed to discuss the dynamics of the magnetic vertex configurations. As a starting point, we will discuss some differences between temporal evolution for systems with and without vacancies. In both cases, the system is initialized considering all the vertices in Type 2, which is a usual initial condition in the literature [19]. This condition results from applying a magnetic field in the diagonal direction of the array so that the magnetic moments are only in one direction aligned on their respective main axes. From now on, we will refer to this initial condition as *Type 2*, regardless of whether the system has vacancies or not. For example, in the case without vacancies corresponds to Type 0V-2, while in the case with one vacancy per-vertex corresponds to type 1V-2.

Fig. 5 shows the temporal evolution of total energy for two cases: without vacancies and with a 30% of vacancies. In both cases, we observe the asymptotic behavior of the energy decreases in time and tends to its minimum with some fluctuations proper of the thermal effect. However, for the situation without vacancies, it is interesting to note an increment in the energy in the first 1×10^3 MC steps,

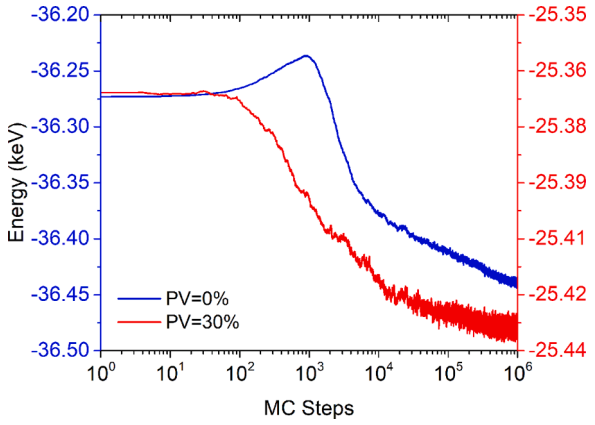


Fig. 5. Temporal evolution of the total energy for a lattice with no vacancies (blue) and 30% vacancies (red). The fixed temperature is $T = 200$ K. (For interpretation of the references to colour in this figure legend, the reader is referred to the web version of this article.)

which is not observed when the system has PV = 30%. The absence of some islands generates a reduction in geometric frustration that facilitates the transition to the lower energy configurations. For example, in vertices with only one vacancy, initialized in Type 1V-2, it is enough with the inversion of one magnetic moment to obtain the vertex with less energy.

Panel (a) of Fig. 6 shows the evolution of the vertex types for the case without vacancies. The system starts with vertices in Type 2, and after an almost stationary transient, the inversion of magnetic configurations is observed. For an intermediate time, the Type 0V-1 and the Type 0V-3 emerge, such that the Type 0V-3 with greater energy than Type 0V-2. This issue explains the increment of the magnetic energy displayed in Fig. 5. The increase in energy is provided by the heat reservoir to which the system is exposed and is part of the dynamics of thermally active systems. Beyond of this intermediate configuration, the Type 0V-2 as well as the Type 0V-3 vertices tend to disappear in favor of the Type 0V-1. The evolution of vertex configurations with vacancies is presented in the panel (b) of Fig. 6. We can observe at the end of the simulation that diverse vertex types corresponding to 1V-1, 0V-1, and 2V-1 have arisen. These vertices possess less energy. However, due to the loss of geometric frustration, the system with vacancies shows higher thermal fluctuations compared to the system without vacancies. This phenomenon is correlated with fluctuations in energy.

Let us extend the discussion on the distribution of the vertices for several percentages of vacancies. In particular, for the following PVs: 0%, 10%, 20%, 30%, 40% and 50%, such that the vacancies are equally distributed between horizontal and vertical islands. We use the same initial condition and temperature of the previous example. For each percentage of vacancies, we considered ten different seeds of random numbers, keeping the same spatial distributions of the vacancies. Table 1 shows the results for the final state of the system (MC steps 1×10^6) averaged over the different samples. It is observed that the vertices with the lowest energy are the most common as expected from a system close to the ground state. For example, the biggest percentages are those associated with types 0V-1, 1V-1, 2V-1, and 2V-2 as well. These states have the lowest energy values, as it is shown in the last column. Of course, this outcome is in concordance with the distribution of vacancies per-vertex presented in Fig. 4. However, the present result allows us to explore how the types of vertex are distributed according to energy for the same number of vacant islands per vertex.

We remark that for the vertex types 0V, 1V, 2V L-shaped, and 2V line-shaped, the statistical weight of the appearance of the excited

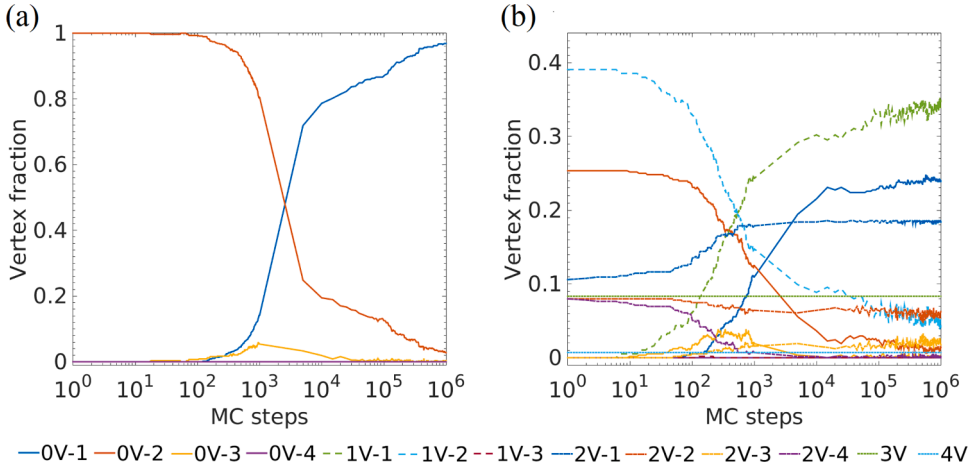


Fig. 6. Temporal evolution of the types of vertices for a ASI lattice with (a) no vacancies and (b) 30% vacancies.The fixed temperature is $T = 200$ K.

Table 1
Distribution of vertex types in terms of the total percentage of system vertices (24 × 24), for several percentages of vacancies (PV). The last column on the right shows the dipolar energy normalized to the magnitude of the Type 0V-1 vertex energy.

Type	0%	10%	20%	30%	40%	50%	ϵ
0V-1	95.486	62.708	41.215	24.618	13.438	5.729	− 1.000
0V-2	4.306	2.257	1.181	0.729	0.278	0.000	− 0.308
0V-3	0.208	0.139	0.139	0.000	0.069	0.000	+ 0.000
0V-4	0.000	0.000	0.000	0.000	0.000	0.000	+ 1.617
1V-1	—	26.701	33.229	34.097	30.035	22.431	− 0.500
1V-2	—	2.813	5.139	4.965	3.646	3.090	− 0.154
1V-3	—	0.000	0.000	0.000	0.000	0.000	+ 0.808
2V-1	—	3.993	10.556	18.507	22.153	24.792	− 0.327
2V-2	—	0.417	3.125	6.111	9.826	11.285	− 0.154
2V-3	—	0.799	1.910	1.875	1.632	1.389	+ 0.154
2V-4	—	0.000	0.035	0.069	0.069	0.208	+ 0.327
3V-1	—	0.174	3.472	8.333	16.667	25.174	—
4V-1	—	0.000	0.000	0.694	2.257	5.904	—
GND	95.486	93.819	88.125	83.333	75.453	64.236	—
GND*	95.486	93.983	91.295	91.603	92.468	93.199	—

states decreases when the percentage of vacancies is raised. The loss of geometric frustration allows the vertices to evolve to their lower energy magnetic configuration. However, this is more pronounced for vertices type 0V and 2V L-shape, than for vertices types 1V and 2V line-shape. This is due to the considerable difference between the minimum energy state and the following energy state. For example, the difference in the case of 0V is $\Delta\epsilon_{0V} = 0.692$ and in the case of 2V L-shape is $\Delta\epsilon_{2V-L} = 0.654$, while for the case of 1V is $\Delta\epsilon_{1V} = 0.346$ and in the case of 2V line-shape is $\Delta\epsilon_{2V-l} = 0.308$. The smaller difference in energy makes transitions between the minimum energy state and the next more probable in the second group. These characteristics can be gathered from Fig. 6 where the cases without vacancies have been compared with the case of 30% vacancies, where the most significant fluctuations are for the 1V-1, 1V-2, 2V-2 and 2V-3 type vertices, as well. Moreover, the last two rows of Table 1 depict the percentage of vertices with the lowest energy states, denoted by GND and GND*. In the case of GND, the statistics are performed over all types of vertices. On the other hand, GND* represents the percentage of vertices in the lowest energy configuration discarding the vertices 3V and 4V. In general, when the system has vacancies, the rate of vertices with the minimum energy configuration is lower than the full case, as indicated by GND*. It is a consequence of the loss of geometric frustration, which allows an increment in the thermal fluctuations.

Let us emphasize that for artificial spin ice systems, the time in which the stationary state can be reached is around ks (hours) [11, 19,49]. The relaxation time depends strongly on the temperature. In particular, in the work of Morley et al. [11], they showed that the time in which the system reaches the stationary state is around 4200 s (more than one hour) at $T = 200$ K. They have also shown that the relaxation time decreases when the temperature increases, and it can be approximated by the Vogel-Fulcher-Tammann law. Our model is based on the aforementioned reference's experimental parameters; consequently, we expect that the system reaches its minimum energy state within times of similar order of magnitude.

Finally, let us also comment that the link of Monte Carlo's steps with physical time is not a simple task [4]. Usually, there is a nonlinear relation between them. In our case, we have used a MC method based on Metropolis algorithm which is a stochastic one that works well in thermal equilibrium since it is based on the canonical ensemble. For this reason, the calculations in the present work focus mainly on thermal equilibrium configurations which can provide an understanding of the basic properties of these systems. Other methods, like Kinetic Monte Carlo [50,51], can provide a connection with real-time.

4. Maximum one vacancy per vertex

In this section, we consider a maximum of one vacancy per vertex in the ASI system. Hence, the number of possible vertex types is reduced to seven. In particular, they are type 0V or 1V. In this circumstance, the maximum percentage of vacancies that can be reached is 25%, which is similar to the scheme presented in Ref[45]. Here we will focus on the possibility of using this reduced system as a magnetic information storage system.

4.1. Magnetic alphabet

The fundamental state of a square ASI without vacancies corresponds to an arrangement of the two possible Type 1 vertex states (0V-1), which alternate, as it is illustrated in Fig. 2(a). When random vacancies are considered, new types of vertices arise, and the system has no periodicity. In principle, one can choose the place of the vacancies and write a message in the lattice.

In principle, one can choose the place of the vacancies and write a message on the lattice. For this purpose, let us associate letters to the minimum energy configurations, taking into account all possible spatial orientations. For the vertices 0V-1 there are two possible configurations. In contrast, for the vertices 1V-1 there are eight possible configurations. It is because a magnetic configuration has two possible states, plus the location within the vertex of the vacancy (4 possible positions). Therefore, there are ten possible letters in their

respective states of local minimum energy. For the case of exited states, we consider just two letters, associated with states with and without vacancies, respectively. These letters form a *magnetic alphabet*. The alphabet is grouped into three subgroups. The first two ones are associated with types 0V-1 and 1V-1: {A, B} and {C, D, E, F, G, H, I, J}, respectively. The letters *K* and *L* represent the excited states {0V-2, 0V-3, 0V-4} and {1V-2, 1V-3}, respectively. The association between the types of vertices and this alphabet is shown in Fig. 7.

An example of how this symbolism can be implemented is given in Fig. 8. Panels (a) and (b) of Fig. 8 show the two possible configurations for the fundamental state, in which the vertices are connected in a defined way. The fundamental state showed in panel (b) presents all the magnetic moments inverted with respect to their corresponding ones in the panel (a). From the alphabet point of view, one can go from one to the other, interchanging the following letters: A ⟷ B, C ⟷ D, E ⟷ F, and J ⟷ I. When the magnetic moment of an island is reversed it immediately affects the other configurations connected to its vertices. Starting from a state of minimum energy spin flips lead to an excited configuration. In the alphabet of Fig. 7 we have defined the letter L for any excited configuration of a vertex without a vacancy and with the letter K for the case with a vacancy. Panels (c) and (d) of Fig. 8 show two examples with excited states with respect to the fundamental state (a). In particular, panel (c) displays one flip in which there are two exited vertices, whereas panel (d) depicts two flips in which there are four exited vertices. Consequently, we can notice that the letters L and K are now on the map, in sequences of two and four, respectively.

The rules of connections, which we will call *grammar*, are detailed in Table 2. The first column represents a central vertex, and the other columns represent the possible closest neighbors in the fundamental state. Consequently, if one wants to write a message using this alphabet, these rules must be respected in order to remain the system in the global minimum energy state. In the following, we will study the stability of these configurations with the temperature.

Finally, let us comment that we have not expanded this alphabet and its grammar for excited vertex configurations because we have not explored excited configurations' stability. However, from an experimental point of view, it was shown that it is possible to change

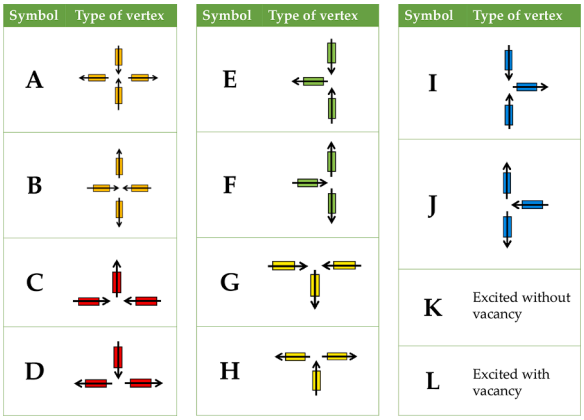


Fig. 7. Magnetic alphabet built from vertex types with maximum one vacancy per vertex.

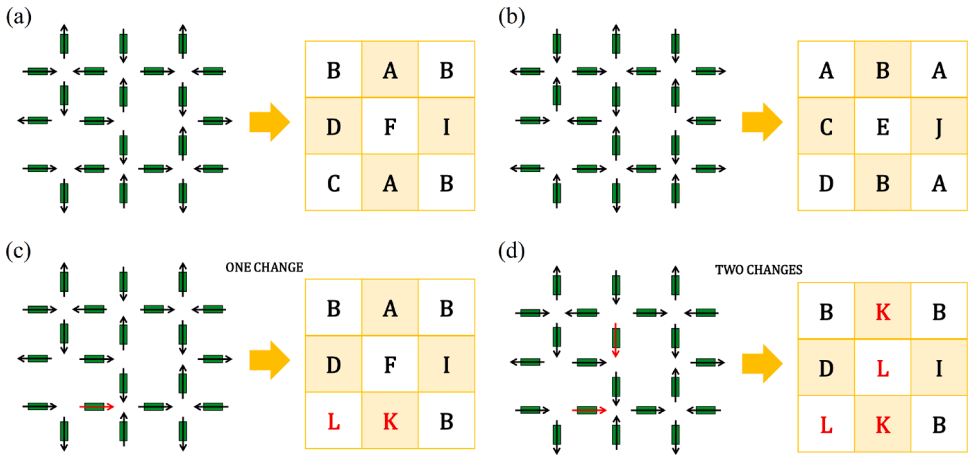


Fig. 8. Examples of how a lattice is mapped with the developed symbology. Panels (a) and (b) show the two possible configurations for the fundamental state. Panel (c) shows the case with one excitations, while panel (d) show case with two excitations. These excited states are respect to the case (a).

Table 2
Alphabet grammar.

Center Vertex	Up	Down	Left	Right
A	B,F,G,J	B,C,F,J	B,C,F,G	B,C,G,J
B	A,E,H,I	A,D,E,I	A,D,E,H	A,D,H,I
C	H	A,E,H,I	A,C,H,I	A,D,E,H
D	G	B,F,G,J	B,C,G,J	B,C,F,G
E	B,C,F,J	B,F,G,J	B,C,G,J	J
F	A,D,E,I	A,E,H,I	A,D,H,I	I
G	A,D,E,I	D	A,D,H,I	A,D,E,H
H	B,C,F,J	C	B,C,G,J	B,C,F,G
I	B,C,F,J	B,F,G,J	F	B,C,F,G
J	A,D,E,I	A,E,H,I	E	A,D,E,H

the direction of the magnetization of each island - in a controlled way - using an MFM equipped with a 2D vector magnet, which opens the possibility to write experimentally different configurations [47]. In principle, with this technique, it is possible to write any configuration within the configuration space. For example, if the number of islands is 22, the number of possible configurations is 10^{22}. Nevertheless, the stability of states with higher energy configurations will be much weaker than the fundamental one. Using this approach, it is possible to write excited configurations, which will have a lifetime of the order of seconds, and then the system will dacay to one of the states with minimal local energy. This can be useful for systems in which we want the written information to disappear after a while. One way to get more stable configurations and then enlarge lifetimes is to decrease the temperature. This is an open problem and could be studied in future works, which would allow us to expand this alphabet.

4.2. Correlations

In this subsection, we analyze the dynamics of the system towards a minimum energy state from the types of vertices and the alphabet points of view. Here, the initial condition is that all the vertices are in the Type 1V-2.

For each seed, the temporal evolution is contrasted with the state that is in the global minimum of the energy, which is vertices 1V-1. Numerically this effective ground state is generated considering one of the two possible ground states of the array without vacancies and dilutes with the corresponding fixed vacancies at the same positions. We repeat this procedure ten times.

For comparison, we defined three different kinds of time correlations. The first one corresponds to the magnetic correlation, C_m, which is the spatial average of the ordered scalar product between the magnetic moments of the template and the magnetic moments in different time steps. The second one corresponds to the vertex correlation, C_v, which is determined by the comparison of the vertices of the template with those of the temporal evolutions for the same spatial locations, such that it is averaged considering all vertices. Here, it is assigned the value 1 if they match in type (1V-1, 1V-2 or 1V-3) or 0 if they do not. Finally, the third correlation corresponds to the letters correlation, C_l, which is similar to vertex correlation but applied to the magnetic alphabet (C, D, E, F, G, H, I or J). In all the cases, the procedure is performed for each MC step and recorded every 4×10^2 MC steps.

Fig. 9 shows the three different correlations as a function of time (MC steps). Panel (a) shows the magnetic correlation, C_m. If the system evolves towards one of the two possible configurations of minimum energy, the final correlation should be $+1$ or -1. However, intermediate values are observed. This reveals that the system evolves towards a mixed state of the two possible configurations, implying fragmented domains with both at minimum energy configurations. It is evident from the curves that neither of the two possible configurations of the fundamental state will dominate, revealing that it is not possible to achieve a global mono-domain with the diluted arrangement when the system starts in Type 2.

The situation of the vertex correlation is entirely different, as it is displayed in the panel (b) of Fig. 9. For the final configuration, the average value of the realization is higher than 0.9 (solid line). The reason for this difference with the magnetic correlation is that the minimum energy states (1V-1) are doubly degenerated (for each spatial orientation). From the magnetic point of view, the correlation between both minimum energy states is negative, and from the vertex point of view, the correlation is 1. The vertex correlation is

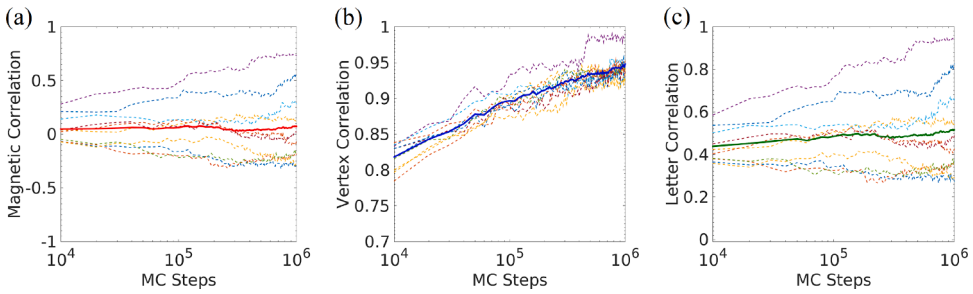


Fig. 9. Correlations as a function of time for: (a) Magnetic correlation, C_m. (b) Vertex correlation, C_v. (c) Letter correlation, C_l. The dashed curves represent the correlation of each sample with the template and the thicker curves are the averages. The temperature is fixed at $T = 200$ K.

directly related to the energy evolution, and the value higher than 0.9 indicates that, for all cases, the system evolves towards close to the minimum energy state. Locally the system evolves through the two possible configurations of minimum energy.

Panel (c) of Figure 9 presents the letter correlation, C_l, as a function of time. A similar result to the magnetic correlation is observed, but with higher values. It is because there is no negative correlation between vertices as it is possible in the case of magnetic correlations. The average over the realizations is close to 0.5 for the whole evolution. This result indicates that, although the system starts with the same initial magnetic conditions, the final result is not predictable from the letters' point of view. The relationship between the magnetic and the letter correlation is direct since each type of vertex has two possible magnetic configurations in the minimum energy state, which correspond to two different letters.

4.3. *Effect of the temperature*

Finally, we study the thermal stability of the magnetic configurations of the system with one vacancy per vertex. Here we use as an initial condition a mixture of the eight vertices Type 1V-1 (see Fig. 7). The considered range of the temperature is from 150 K to 400 K, with intervals of 50 K was considered. The system was left to evolve for 2×10^5 MC steps because the system thermalizes around 2×10^4 MC steps. From a technical point of view, we run ten independent realizations, and the magnetic configurations were recorded every 5×10^2 MC steps.

Fig. 10 illustrates the time average of the correlations as a function of temperature. We can observe that the three correlations show strong similarities. We can recognize that the correlations decrease when the temperature increases. The vertex correlation remains higher in comparison with the other. The letter correlation present intermediate values when compared with others, this is an indication that fluctuation among symbols is higher that fluctuation among vertices. On the other hand, the magnetic correlation is the lowest one, as a result of variations in the direction of the magnetic moments along the island's axis. We remark that in three cases the correlation decays with a law $C_j(T) \approx C_{0,j} - \alpha_j T^{\beta_j}$, such that $C_{0,j} \approx 1.0$, α_j are small positive values and $(\beta_m, \beta_v, \beta_l) \approx (6.63, 5.76, 4.69)$.

These results indicate that an ASI system with vacancies will maintain its magnetic order with minor fluctuations when it is allowed to evolve from the fundamental state, even at relatively high values of the temperature.

5. Final remarks

We have characterized the distributions of vertex types in a square array of ASI with different percentages of vacant islands. We have ordered the vertex types according to the number of vacancies and energy levels of the possible magnetic configurations. From a dynamic point of view, the system with vacancies reaches thermal equilibrium in less time (Monte Carlo steps) due to the loss of geometric frustration of the system. However, this loss of frustration generates more thermal fluctuations than in the case without vacancies. Therefore, configurations with higher energy contributions coming from the vertices present a more significant probability of being observed. A more in-depth analysis of the thermal activation temperature as a function of the percentage of vacant islands will be done in future works.

Let us also remark that in several works on square ASI, the system evolves from an initial Type 2 conditions to large domains of Type 1 vertices separated by the so-called Dirac strings. Even more, the system can reach any of the two fundamental states, which is a single monodomain [18,19]. On the contrary, in the diluted systems, we have observed that a single monodomain is not possible due to the fragmentation of the lattice by the vacancies. Nevertheless, when any of the fundamental states is reached in diluted systems, it is robust in a wide range of temperatures. This issue is an advantage in order to observe a wide variety of magnetic textures. In this sense,

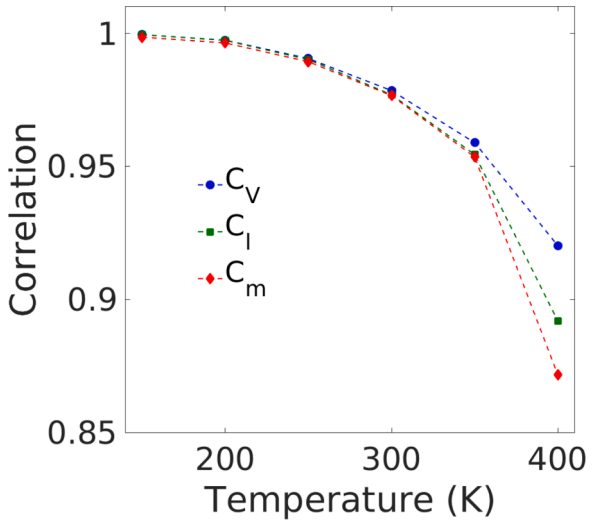


Fig. 10. Magnetic correlation, vertex correlation and letter correlation as a function of temperature.

we have been able to define an alphabet with its own writing rules.

Finally, from an information systems point of view, since the magnetic configuration states on ASIs with vacant islands remain stable for a broad range of temperatures, we can infer that magnetic memory systems based on ASI-type arrays open the possibilities to a new generation of information storage systems.

Declaration of Competing Interest

The authors declare that they have no known competing financial interests or personal relationships that could have appeared to influence the work reported in this paper.

Acknowledgments

FB acknowledges the financial support from CONICYT fellowship and thanks to Guidobeth Saez (UFRO) for useful discussions. PD thanks DIUFRO Project No. DI18-0066. PD and EEV acknowledge partial financial from FONDECYT 1190036. PD, DL and LMP acknowledge partial financial from FONDECYT 1180905. DL and EEV acknowledge partial financial support from Centers of Excellence with BASAL/CONICYT financing, Grant AFB180001, CEDENNA. This research was partially supported by the supercomputing infrastructure at the NLHPC (ECM-02). Finally, DL sincerely acknowledges the Materials and Condensed Matter Physics Group at the University of Glasgow, where the initial and further stimulating discussions on the ASI topic emerged along with his research stay in Scotland.

References

[1] C. Nisoli, R. Moessner, P. Schiffer, Colloquium: artificial spin ice: designing and imaging magnetic frustration, Rev. Mod. Phys. 85 (2013) 1473–1490, https://doi.org/10.1103/revmodphys.85.1473.
[2] L.J. Heyderman, R.L. Stamps, Artificial ferroic systems: novel functionality from structure, interactions and dynamics, J. Phys. Condens. Matter 25 (2013) 36, https://doi.org/10.1088/0953-8984/25/36/363201.
[3] I. Gilbert, C. Nisoli, P. Schiffer, Frustration by design, Phys. Today 69 (2016) 55–59, https://doi.org/10.1063/PT.3.3237.
[4] D.P. Landau, K. Binder, A guide to Monte Carlo simulations in statistical physics, third ed, Cambridge University Press, UK, 2000.
[5] A.P. Ramirez, Strongly geometrically frustrated magnets, Annu. Rev. Mater. Sci. 24 (1994) 453–480, https://doi.org/10.1146/annurev.ms.24.080194.002321.
[6] M.J. Harris, S.T. Bramwell, D.F. McMorrow, T. Zeiske, K.W. Godfrey, Geometrical frustration in the ferromagnetic pyrochlore $Ho_2 Ti_2 O_7$, Phys. Rev. Lett. 79 (1997) 2554–2557, https://doi.org/10.1103/PhysRevLett.79.2554.
[7] L. Pauling, The Nature of the Chemical Bond and the Structure of Molecules and Crystals: An Introduction to Modern Structural Chemistry, third ed, Cornell University Press, USA, 1960.
[8] A.P. Ramirez, A. Hayashi, R.J. Cava, R. Siddharthan, B.S. Shastry, Zero-point entropy in 'spin ice', Nature 399 (1999) 333–335, https://doi.org/10.1038/20619.
[9] R.F. Wang, C. Nisoli, R.S. Freitas, J. Li, W. McConville, B.J. Cooley, M.S. Lund, N. Samarth, C. Leighton, V.H. Crespi, P. Schiffer, Artificial "spin ice" in a geometrically frustrated lattice of nanoscale ferromagnetic islands, Nature 439 (2006) 303–306, https://doi.org/10.1038/nature04447.
[10] L. Anghinolfi, H. Luetkens, J. Perron, M.G. Flokstra, O. Sendetskyi, A. Suter, T. Prokscha, P.M. Derlet, S.L. Lee, L.J. Heyderman, Thermodynamic phase transitions in a frustrated magnetic metamaterial, Nat. Commun. 6 (2015) 8278, https://doi.org/10.1038/ncomms9278.
[11] S.A. Morley, D.A. Venero, J.M. Porro, S.T. Riley, A. Stein, P. Steadman, R.L. Stamps, S. Langridge, C.H. Marrows, Vogel-fulcher-tammann freezing of a thermally fluctuating artificial spin ice probed by x-ray photon correlation spectroscopy, Phys. Rev. B 95 (2017) 1–6, https://doi.org/10.1103/PhysRevB.95.104422.
[12] D. Shi, Z. Budrikis, A. Stein, S.A. Morley, P.D. Olmsted, G. Burnell, C.H. Marrows, Frustration and thermalization in an artificial magnetic quasicrystal, Nature Phys. 14 (2018) 309–314, https://doi.org/10.1038/s41567-017-0009-4.
[13] R.P. Loreto, F.S. Nascimento, R.S. Gonçalves, J. Borme, J.C. Cezar, C. Nisoli, A.R. Pereira, C.I.L. de Araujo, Experimental and theoretical evidences for the ice regime in planar artificial spin ices, J. Phys.: Condens. Matter 31 (2019) 25301, https://doi.org/10.1088/1361-648x/aaeeef.
[14] X. Zhang, Y. Lao, J. Sklenar, N.S. Bingham, J.T. Batley, J.D. Watts, C. Nisoli, C. Leighton, P. Schiffer, Understanding thermal annealing of artificial spin ice, APL Mater. 7 (2019) 111112, https://doi.org/10.1063/1.5126713.
[15] G.-W. Chern, C. Reichhardt, C. Nisoli, Realizing three-dimensional artificial spin ice by stacking planar nano-arrays, Appl. Phys. Lett. 104 (2014) 013101, https://doi.org/10.1063/1.4861118.
[16] E. Östman, H. Stopfel, I.-A. Chioar, U.B. Arnalds, A. Stein, V. Kapaklis, B. Hjörvarsson, Interaction modifiers in artificial spin ices, Nat. Phys. 14 (2018) 375–379, https://doi.org/10.1038/s41567-017-0027-2.
[17] G. Möller, R. Moessner, Artificial square ice and related dipolar nanoarrays, Phys. Rev. Lett. 96 (2006) 237202, https://doi.org/10.1103/PhysRevLett.96.237202.
[18] J.P. Morgan, A. Stein, S. Langridge, C.H. Marrows, Thermal ground-state ordering and elementary excitations in artificial magnetic square ice, Nat. Phys. 7 (2011) 75–79, https://doi.org/10.1038/nphys1853.
[19] A. Farhan, P.M. Derlet, A. Kleibert, A. Balan, R.V. Chopdekar, M. Wyss, J. Perron, A. Scholl, F. Nolting, L.J. Heyderman, Direct observation of thermal relaxation in artificial spin ice, Phys. Rev. Lett. 111 (2013) 1–5, https://doi.org/10.1103/PhysRevLett.111.057204.
[20] C. Castelnovo, R. Moessner, S.L. Sondhi, Spin ice, fractionalization, and topological order, Annu. Rev. Condens. Matter Phys. 3 (2012) 35–55, https://doi.org/10.1146/annurev-conmatphys-020911-125058.
[21] Y. Perrin, B. Canals, N. Rougemaille, Extensive degeneracy, coulomb phase and magnetic monopoles in artificial square ice, Nature 540 (2016) 410–413, https://doi.org/10.1038/nature20155.
[22] N. Keswani, P. Das, Magnetization reversal and emergent magnetic monopole-like state in square artificial spin ice vertex with defects, AIP Adv 8 (2018) 101501, https://doi.org/10.1063/1.5042803.
[23] A. Farhan, M. Saccone, C.F. Petersen, S. Dhuey, R.V. Chopdekar, Y.-L. Huang, N. Kent, Z. Chen, M.J. Alava, T. Lippert, A. Scholl, S. van Dijken, Emergent magnetic monopole dynamics in macroscopically degenerate artificial spin ice, Sci. Adv. 5 (2019) 1–9, https://doi.org/10.1126/sciadv.aav6380.
[24] C. Donnelly, M. Guizar-Sicairos, V. Scagnoli, M. Holler, T. Huthwelker, A. Menzel, I. Vartiainen, E. Müller, E. Kirk, S. Gliga, J. Raabe, L.J. Heyderman, Element-specific x-ray phase tomography of 3D structures at the nanoscale, Phys. Rev. Lett. 114 (2015) 115501, https://doi.org/10.1103/PhysRevLett.114.115501.
[25] Y. Liu, S. Kempinger, R. He, T.D. Day, P. Moradifar, S.Y. Yu, J.L. Russell, V.M. Torres, P. Xu, T.E. Mallouk, S.E. Mohney, N. Alem, N. Samarth, J.V. Badding, Confined chemical fluid deposition of ferromagnetic metalattices, Nano Lett. 18 (2018) 546–552, https://doi.org/10.1021/acs.nanolett.7b04633.
[26] A. Mistonov, I.S. Dubitskiy, I.S. Shishkin, N.A. Grigoryeva, A. Heinemann, N.A. Sapoletova, G.A. Valkovskiy, S.V. Grigoriev, Magnetic structure of the inverse opal-like structures: small angle neutrondiffraction and micromagnetic simulations, J. Magn. Magn. Mater. 477 (2019) 99–108, https://doi.org/10.1016/j.jmmm.2019.01.016.
[27] A. May, M. Hunt, A.V.D. Berg, A. Hejazi, S. Ladak, Realisation of a frustrated 3D magnetic nanowire lattice, Commun. Phys. 2 (2019) 13, https://doi.org/10.1038/s42005-018-0104-6.

[28] H. Arava, P.M. Derlet, J. Vijayakumar, J. Cui, N.S. Bingham, A. Kleibert, L.J. Heyderman, Computational logic with square rings of nanomagnets, Nanotechnology 29 (2018) 265205, https://doi.org/10.1088/1361-6528/aabbc3.
[29] F. Caravelli, C. Nisoli, Logical gates embedding in artificial spin ice, New J. Phys. 22 (2020) 103052, https://doi.org/10.1088/1367-2630/abbf21.
[30] P. Gypens, J. Leliaert, B.V. Waeyenberge, Balanced magnetic logic gates in a kagome spin ice, Phys. Rev. Applied 9 (2018) 034004, https://doi.org/10.1103/PhysRevApplied.9.034004.
[31] H. Arava, N. Leo, D. Schildknecht, J. Cui, J. Vijayakumar, P.M. Derlet, A. Kleibert, L.J. Heyderman, Engineering relaxation pathways in building blocks of artificial spin ice for computation, Phys. Rev. Applied 11 (2019) 054086, https://doi.org/10.1103/PhysRevApplied.11.054086.
[32] G.W. Chern, Magnetotransport in artificial kagome spin ice, Phys. Rev. Applied 8 (2017) 064006, https://doi.org/10.1103/PhysRevApplied.8.064006.
[33] S.H. Skjærvø, C.H. Marrows, R.L. Stamps, L.J. Heyderman, Advances in artificial spin ice, Nat. Rev. Phys. 2 (2020) 13–28, https://doi.org/10.1038/s42254-019-0118-3.
[34] C. Nisoli, V. Kapaklis, P. Schiffer, Deliberate exotic magnetism via frustration and topology, Nat. Phys. 13 (2017) 200–203, https://doi.org/10.1038/nphys4059.
[35] A. Ortiz-Ambriz, C. Nisoli, C. Reichhardt, C.J.O. Reichhardt, P. Tierno, Colloquium: ice rule and emergent frustration in particle ice and beyond, Rev. Mod. Phys. 91 (2019) 041003, https://doi.org/10.1103/RevModPhys.91.041003.
[36] S. Lendinez, M.B. Jungfleisch, Magnetization dynamics in artificial spin ice, J. Phys. Condens. Matter 32 (2020) 013001, https://doi.org/10.1088/1361-648X/ab3e78.
[37] S. Gliga, E. Iacocca, O.G. Heinonen, Dynamics of reconfigurable artificial spin ice: toward magnonic functional materials, APL Mater 8 (2020) 040911, https://doi.org/10.1063/1.5142705.
[38] Y. Qi, T. Brintlinger, J. Cumings, Direct observation of the ice rule in an artificial kagome spin ice, Phys. Rev. B 9 (2008) 094418, https://doi.org/10.1103/PhysRevB.77.094418.
[39] G. Moeller, R. Moessner, Magnetic multipole analysis of kagome and artificial spin-ice dipolar arrays, Phys. Rev. B 80 (2009) 140409, https://doi.org/10.1103/PhysRevB.80.140409.
[40] S. Ladak, D.E. Read, G.K. Perkins, L.F. Cohen, W.R. Branford, Direct observation of magnetic monopole defects in an artificial spin-ice system, Nat. Phys. 6 (2010) 359–363, https://doi.org/10.1038/nphys1628.
[41] E. Mengotti, L.J. Heyderman, A.F. Rodríguez, F. Nolting, R.V. Hügli, H.B. Braun, Real-space observation of emergent magnetic monopoles and associated dirac strings in artificial kagome spin ice, Nat. Phys. 7 (2011) 68–74, https://doi.org/10.1038/nphys1794.
[42] V. Kapaklis, U.B. Arnalds, A. Harman-Clarke, E.T. Papaioannou, M. Karimipour, P. Korelis, A. Taroni, P.C.W. Holdsworth, S.T. Bramwell, B. Hjorvarsson, Melting artificial spin ice, New J. Phys. 14 (2012) 035009, https://doi.org/10.1088/1367-2630/14/3/035009.
[43] V. Kapaklis, U.B. Arnalds, A. Farhan, R.V. Chopdekar, A. Balan, A. Scholl, L.J. Heyderman, B. Hjorvarsson, Thermal fluctuations in artificial spin ice, Nat. Nanotechnol. 9 (2014) 514–519, https://doi.org/10.1038/nnano.2014.104.
[44] M.J. Morrison, T.R. Nelson, C. Nisoli, Unhappy vertices in artificial spin ice: new degeneracies from vertex frustration, New J. Phys 15 (2013) 045009, https://doi.org/10.1088/1367-2630/15/4/045009.
[45] A. Libál, D.Y. Lee, A. Ortiz-Ambriz, C. Reichhardt, C.J.O. Reichhardt, P. Tierno, C. Nisoli, Ice rule fragility via topological charge transfer in artificial colloidal ice, Nat. Commun. 9 (2018) 4146, https://doi.org/10.1038/s41467-018-06631-1.
[46] I. Gilbert, Y. Lao, I. Carrasquillo, L. O'brien, J.D. Watts, M. Manno, C. Leighton, A. Scholl, C. Nisoli, P. Schiffer, Emergent reduced dimensionality by vertex frustration in artificial spin ice, Nat. Phys. 12 (2016) 162–165, https://doi.org/10.1038/nphys3520.
[47] Y.-L. Wang, Z.-L. Xiao, A. Snezhko, J. Xu, L.E. Ocola, R. Divan, J.E. Pearson, G.W. Crabtree, W.K. Kwok, Rewritable artificial magnetic charge ice, Science 352 (2016) 962–966, https://doi.org/10.1126/science.aad8037.
[48] A. Aharoni, Demagnetizing factors for rectangular ferromagnetic prisms, J. Appl. Phys. 13 (1998) 3432, https://doi.org/10.1063/1.367113.
[49] J.M. Porro, S.A. Morley, D.A. Venero, R. Macedo, M.C. Rosamond, E.H. Linfield, R.L. Stamps, C.H. Marrows, S. Langridge, Magnetization dynamics of weakly interacting sub-100 nm square artificial spin ices, Sci. Rep. 9 (2019) 19967, https://doi.org/10.1038/s41598-019-56219-y.
[50] A.B. Bortz, M.H. Kalos, J.L. Lebowitz, A new algorithm for monte carlo simulation of ising spin systems, J. Comput. Phys. 17 (1975) 10–18, https://doi.org/10.1016/0021-9991(75)90060-1.
[51] A.P.J. Jansen, An Introduction to Kinetic Monte Carlo Simulations of Surface Reactions, First ed, Springer, Germany, 2012.